Bio- and Chemically Synthesized ZnO Nanoparticles for Textile Wastewater Treatment and Phytotoxicity Alleviation in *Vigna radiata*

Fatima Batool[a,b], Muhammad Zubair[b], Faisal Mahmood[a], Muhammad Shahid[c], Tanvir Shahzad[a], Weitao Liu[d], Sabir Hussain[a]*, Aman Ullah[b*]

[a] *Department of Environmental Sciences, Government College University Faisalabad, Faisalabad, 38000, Pakistan*

[b] *Department of Agricultural, Food & Nutritional Science, Faculty of ALES, University of Alberta 4-10 Agriculture/Forestry Centre Edmonton, AB, T6G 2P5*

[c] *Department of Bioinformatics and Biotechnology, Government College University Faisalabad, Faisalabad, 38000, Pakistan*

[d] *MOE Key Laboratory of Pollution Processes and Environmental Criteria, College of Environmental Science and Engineering, Nankai University, Tianjin 300350, China*

*: *Correspondence authors*

sabirghani@gmail.com; sabir.hussain@gcuf.edu.pk

ullah2@ualberta.ca

S.1 Material and Methods

S.1.1 Decolorization of dyes at their different concentrations

After optimization, the optimum concentration of nanoparticles was used for the decolorization of MB, CR, RB-5, MG, and RR-2 at 25, 50, and 75 ppm. For this purpose, the optimum concentration of ZnO-NPs was mixed to each dye solution (n=3) and placed for solar incubation. At specific time intervals, small aliquots were taken from each sample and subjected to spectrophotometry to estimate the effect of the optimum dosage of NPs on decolorizing dyes at different concentrations.

S.1.2 Decolorization of dyes under different incubation conditions

The potential of ZnO-NPs was estimated for removal of dyes (50 ppm) under dark and light condition. A 40 W UV black light florescent bulb, white LED light, and nautural sunlight conditions (Experimental Month= June; Solar irradiance range= 800 to 1000 W m^{-2}; Experimental site= GCUF, Faislabad, Pakistan) were used as a light sources. Samples with different dye solutions (50 ppm concentration; n=3) and optimum concentrations of nanoparticles were placed under each light source for a particular time. The 2 mL of aliquots was taken from each sample, centrifuged (7000 rpm) and the decolorization % was estimated using a spectrophotometer at specific wavelengths of each dye.

S.1.3 Decolorization of dyes in presence of reducing agent

The optimum dosage of ZnO-NPs was used for the decolorization of tested dyes using $NaBH_4$ as a reducing agent. After adding $NaBH_4$ (3:1) and nanomaterials to each dye solution (n=3), the reaction solution was placed in dark. Approximately 2 mL of sample were taken from each reaction

solution after particular time intervals and subjected to UV-visible spectrophotometer to determine the rate of degradation of each dye.

S.2 Results

S.2.1 Decolorization of dyes at their different concentrations

After optimization, the optimum dosage of ZnO-NPs was used for the decolorization of azo dyes at different concentrations (**Fig. S1**). The maximum decolorization with the application of ZnO(B)-NPs was observed for CR dye at a concentration of 25 ppm, followed by MG, MB, RB-5, and RR-2. A similar trend was observed with the treatment of ZnO(C)-NPs, but their potential was found to be less than that of the biologically synthesized counterparts. The decolorization potential of the nanomaterials decreased with increasing dye concentration. At 50 ppm, the maximum decolorization was again observed in CR, followed by MG, MB, RB-5 and RR-2 by ZnO(B)-NPs. In the case of ZnO(C)-NPs, the removal efficiencies for MB, RR-2, and RB-5 were similar; however, after 1 h, the following decolorization rate was observed: CR>MG > MB>RB-5 > RR-2. This increasing decolorization in CR, MG, and MB might be due to the simple chromophoric structure and azo bonds, which are easily attached by hydroxyl and superoxide radicals generated by ZnO-NPs. Conversely, reactive dyes have more complex structures (sulfonate aromatic group) and bonds, making them difficult to remove.[1] The potential of nanomaterials was significantly reduced at 75 ppm of dye, and the decolorization trend of both nanomaterials for MB, RR-2, and RB-5 were similar and lower than that at 25 and 50 ppm. The findings of this experiment are aligned with the studies of Bagheri et al.[2], Farouq et al.[3], Shubha et al.[4]. They reported that as the dye concentration increased, the transparency of the solutions decreased, which absorbed UV light from the sun, making it less available for catalysts. Meanwhile, it also reduced the production of hydroxyl ions, which are required for the photocatalytic degradation of dyes.[4] Bagheri et al.[2]

reported that dye decolorization may occurs by the transfer of electrons from the surface of ZnO-NPs to dye molecules. As the dye concentration increases, the production of electrons and holes may decrease, which can reduce the decolorizing potential of the NPs.

The results of this experiment were further confirmed by heat map and principal component analysis. PCA of variables (**Fig. S1G**) confirmed the results, where Dim1 contributed approximately 87.9 % and Dim2 approximately 6.2% of the variance. This indicates that the decolorization of each dye follows a uniform kinetic trend, and the closeness of the vectors suggests that they are positively correlated. In the PCA of treatments (**Fig. S1H**), experimental variables were grouped based on dye concentration (25, 50, and 75 ppm). The 75 ppm confidence ellipses along Dim1 and Dim2 indicated that the dye concentration had a significant impact on the degradation pathway compared to lower concentrations. The heatmap (**Fig. S1I**) shows a high degree of similarity in the degradation rate of all tested dyes, while its hierarchical clustering identifies the role of catalysts in degrading different concentrations of dyes in different time intervals. In the heatmap, blue indicates the least decolorization, and red indicates the maximum decolorization of dyes.

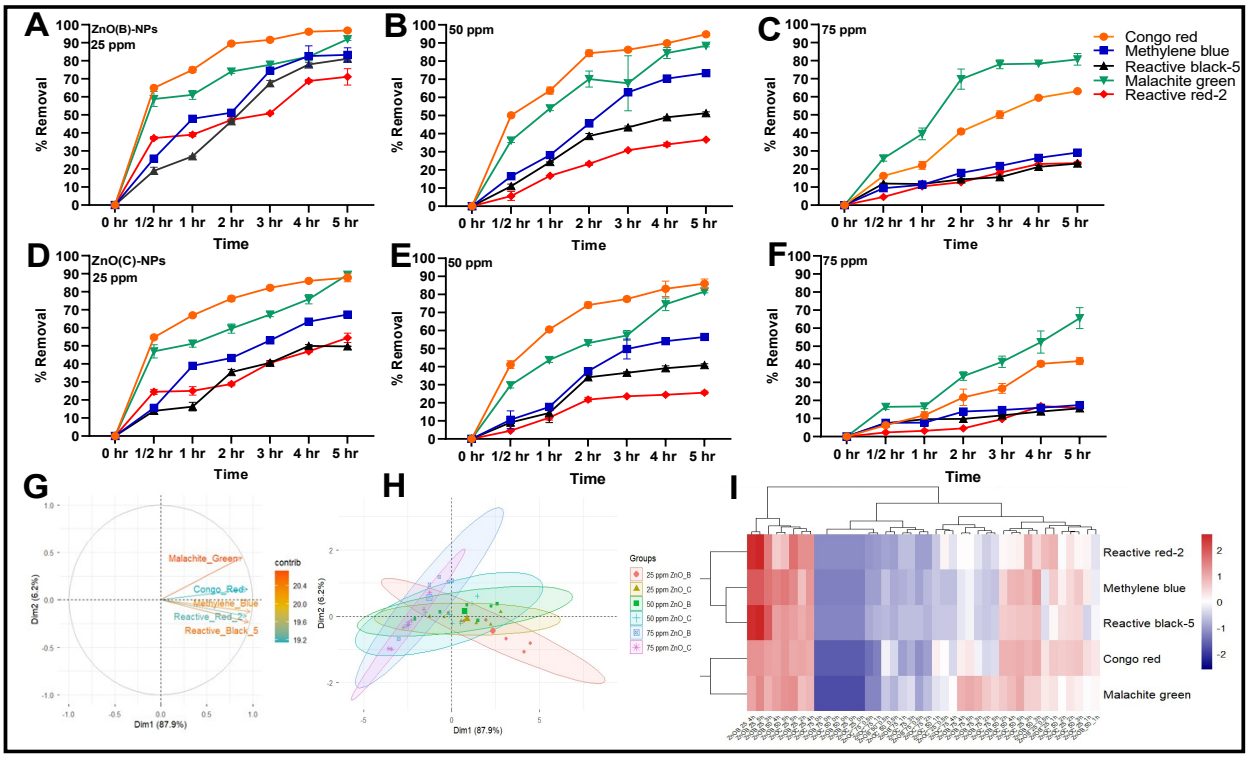

Fig. S1 Decolorization of azo dyes using optimized concentrations of prepared ZnO-NPs at 25, 50, and 75 ppm of dye from simulated wastewater. Line graphs represent the decolorization of dyes while PCA and heat map demonstrate the multivariant analysis. Error bars represent the standard deviation (n=3)

S.2.2 Decolorization of dyes under different incubation conditions

Fig. S2 shows the potential of ZnO(B) and ZnO(C) NPs in decolorizing different azo dyes in the dark and under different light sources. The minimum decolorization was observed during dark incubation compared to other light sources. It might be due to the activation of adsorption process rather than photocatalytic activity. Under UV-light incubation, the maximum decolorization for all dyes were observed, with CR and MG showing decolorization of more than 90 %. Conversely, the presence of white light moderately decolorized the azo dyes.

Meanwhile, sunlight incubation resulted in high removal of dyes comparable to the decolorizing potential of UV light because of its broad wavelength range. Under light conditions, ZnO-NPs may act as photocatalysts and produced reactive oxygen species such as hydroxyl and superoxide radicals[5,6], which may help in oxidative degradation of dyes into simple compounds as reported in peroxide-mediated oxidation systems.[7] The findings of the whole study are compared with other studies and summarized in **Table S1.** Basically, electrons from valance band (VB) triggered to the conductance band (CB) on exposure of light energy that is more than the band gap of ZnO-NPs (Equation 1).[8]

$$ZnO + h\nu \rightarrow ZnO + h^{+}\text{ (valance band VB)} + e^{-}\text{ (conductance band CB)} \ldots. (1)$$

Then, the oxygenation of water molecules and surface hydroxyl groups occurs and is converted into hydroxyl radicals (Equations 2 and 3).

$$h^{+}(VB) + H_2O \rightarrow OH\bullet + H^{+} \ldots. (2)$$

$$h^{+} + OH \rightarrow OH\bullet \ldots. (3)$$

On the other hand, superoxide radicals were also produced when oxygen in the dissolved form reacted with the electrons of the conduction band (Equation 4).

$$e\ (CB) + O_2 \rightarrow O_2^{\bullet -} \ldots. (4)$$

These reactive oxygen species in the form of superoxide and hydroxyl radicals degrade the dyes into simple molecules and less harmful compounds such as CO_2, H_2O, and inorganic ions (Equation 5).[9]

$$Dye + ROS \rightarrow CO_2 + H_2O + \text{inorganic ions} \ldots. (5)$$

During multivariate analysis, the PCA analysis of dye decolorization (**Fig. S2I**) showed that DIM 1 contributed approximately 87.9% and DIM 2 approximately 6.2% of the variance. All the dyes exhibited positive relationships, which suggest that they follow specific degradation trends.

Additionally, the PCA analysis in **Fig. S2J** shows the impact of light sources on the decolorization of each dye. The sun and UV light were toward DIM 1, showing more decolorization, while dark and white light were toward DIM 2, showing less decolorization of dyes, which further confirmed our results. The heatmap analysis (**Fig. S2K**) confirmed that each incubation condition had a significant influence on dye decolorization. In it, UV and sunlight are represented by red color showing maximum decolorization of dyes, while blue color is attributed to dark and white light, showing the least decolorization.

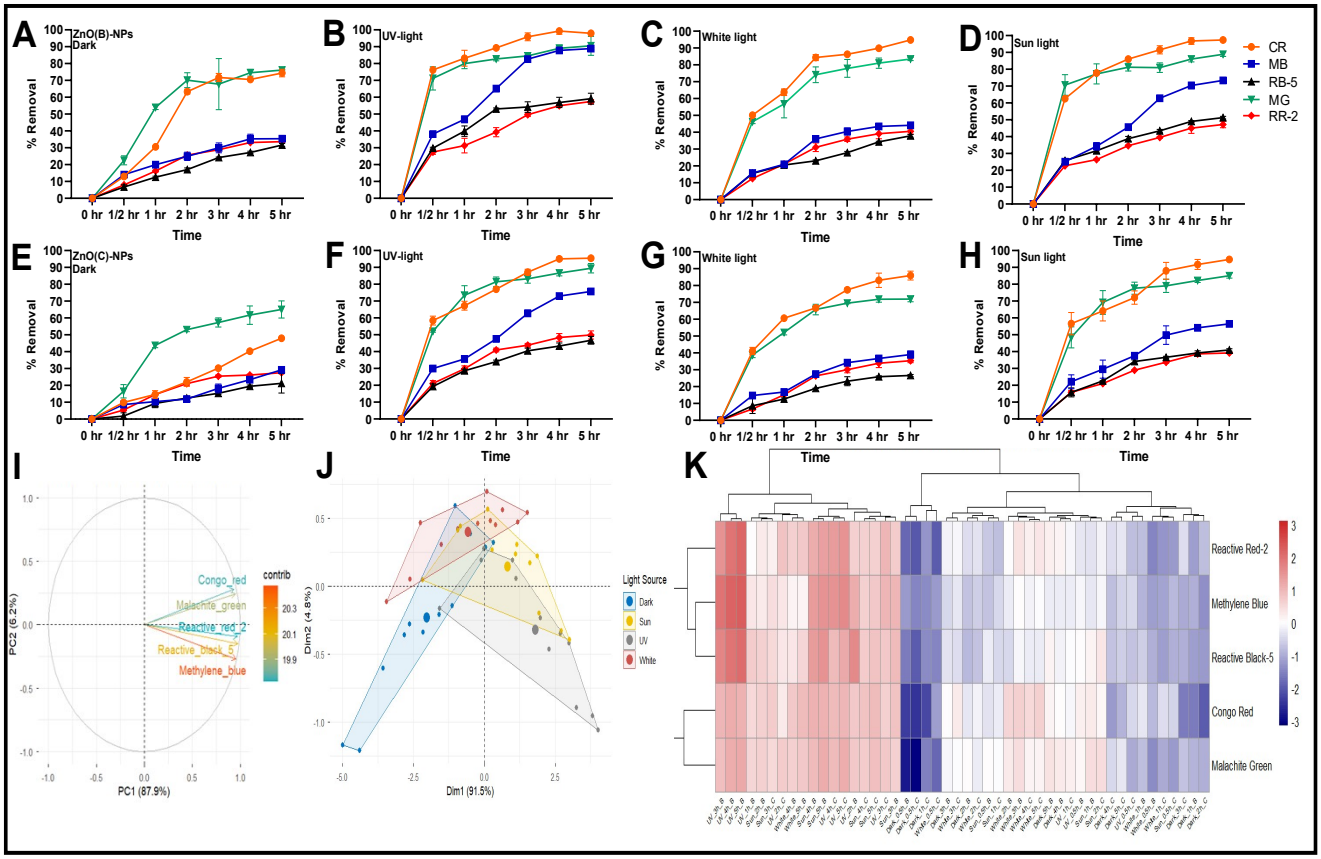

Fig. S2 Decolorization of azo dyes from synthetic wastewater using ZnO-NPs under dark, UV light, white light, and sunlight conditions. Line graphs represent the decolorization of dyes while PCA and heat map demonstrate the multivariant analysis. Error bars are the standard deviation (n=3)

S.2.3 Decolorization of dyes in presence of reducing agent

The synergistic potential of ZnO(C) and ZnO(B) NPs, with and without $NaBH_4$, was also assessed for the decolorization of dyes in synthetic wastewater (**Fig. S3**). It was noticed that maximum decolorization was demonstrated by the treatment of NPs+$NaBH_4$. Al-Shehri et al.[10] reported that the process of removing dyes is increased with the addition of $NaBH_4$ and NPs. Additionally, decolorization was most prominent in CR, followed by MG, MB, and RR-2, and it increased with time. CR, MG, and MB showed the highest removal across all the treatments whereas RR-2 and RB-5 showed slower degradation due to their complex molecular structures. It was observed that biosynthesized ZnO-NPs showed more potential with $NaBH_4$ as compared to their chemically synthesized counterparts. Basically, the addition of $NaBH_4$ increases the reduction of azo bonds which breakdown the structure of azo dyes.[11] This process produced intermediate byproducts which may be further degraded by nanomaterials. This mutual interaction between the catalyst and reducing agent may also be responsible for the increased removal rate of dyes.

Further, PCA analysis (**Fig. S3F**) showed the positive loading of all dyes along Dim1 (92.6%) which proves the behavior of dye degradation is controlled mainly by one common factor, namely catalytic activity. Congo red and malachite green had relatively higher contributions, indicating that they were more responsive to the applied treatments than the others. The PCA of the treatments (**Fig. S3G**) showed that ZnO(B) and ZnO(B)+$NaBH_4$ were placed towards the positive side of Dim1, which shows a better degradation capacity, while $NaBH_4$ was on the negative side, indicating that it is not an efficient catalyst. Intermediate positions were taken by ZnO(C) and ZnO(C)+$NaBH_4$, indicating that they were moderately effective. The heatmap analysis (**Fig. S3H)** showed the degradation of dyes using reducing agent under specific time intervals. In the map, red indicates a positive relationship (more decolorization) and blue indicate a negative relationship

(less decolorization). The application of ZnO(B)-NPs with reducing agent outperformed the other catalyst by showing more red hues.

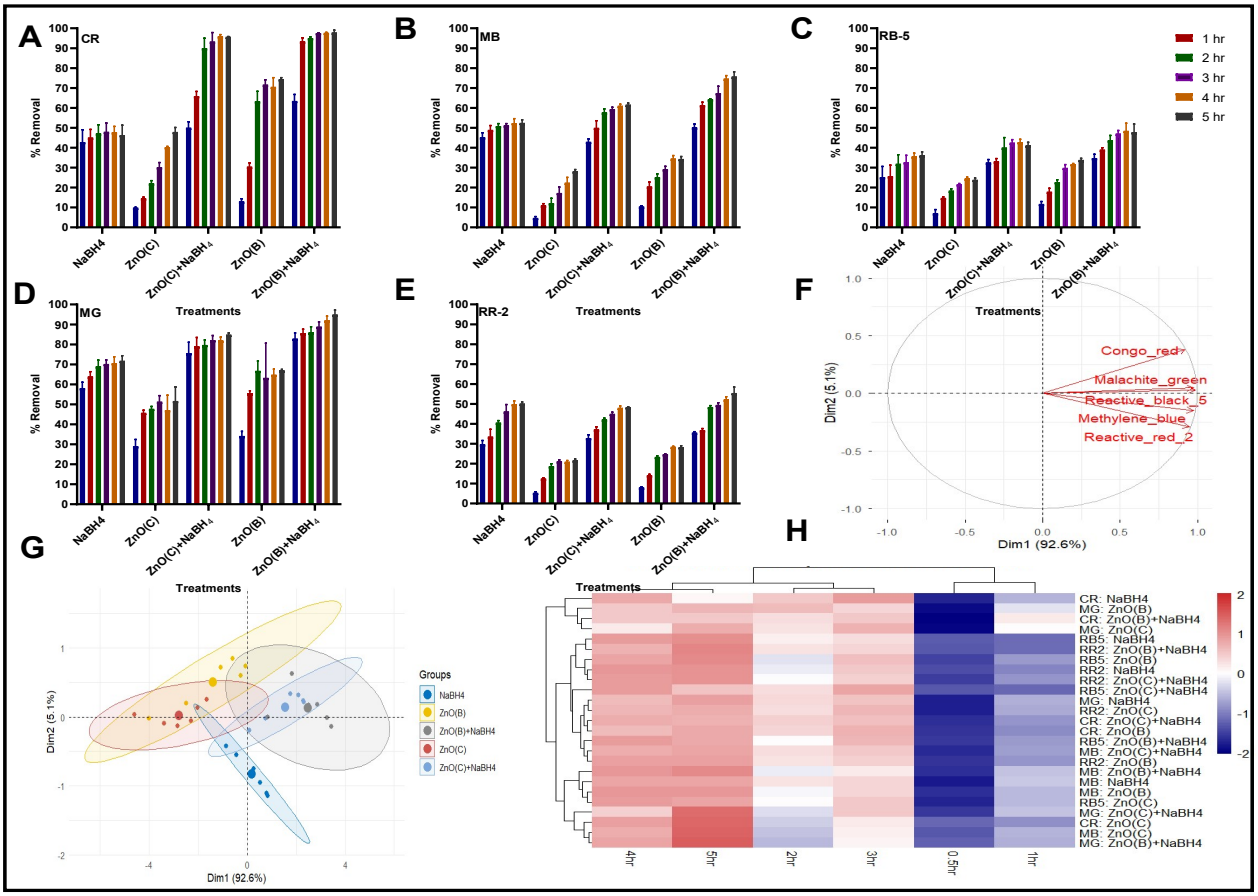

Fig. S3 Decolorization of azo dyes from synthetic wastewater using ZnO-NPs with and without reducing agent ($NaBH_4$). Bar graphs represent the decolorization of dyes while PCA and heat map demonstrate the multivariant analysis. Error bars represent the standard deviation (n=3)

162 **Figures**

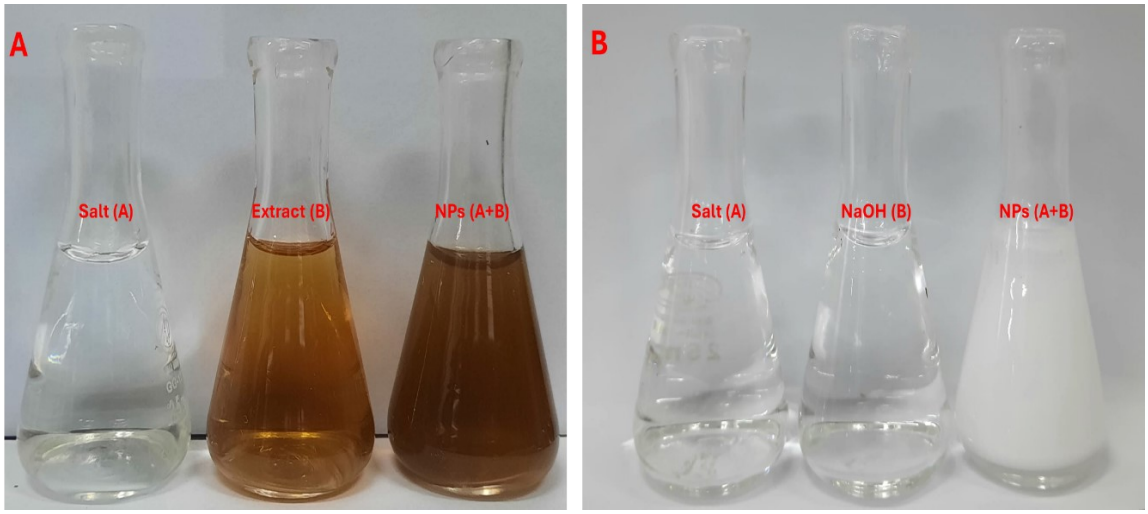

163

164 **Fig. S4** Visual representation of change in color from yellow to brownish during bio (A) and

165 transparent to milky during chemical (B) synthesis of ZnO-NPs

166

168

169 **Table S1** Comparison of decolorization of dyes using ZnO-NPs with other studies

Catalyst	Synthesis Route	Pollutant	Catalyst Conc.	Pollutant Conc.	Incubation Source	Removal Efficiency	Reference
ZnO-NPs	Microbial via *Pseudochrobactrum* sp. and Chemically using NaOH	Brilliant Blue R (BB-R), Brilliant Yellow (BY), Reactive Red 2 (RR-2), and Reactive Black 5 (RB-5)	10 mg 10 mL^{-1}	200 mg L^{-1}	Sun light	BB-R (83.2%), BY (83.1%), RR-2 (88.8%), and RB-5 (95.2%) by biosynthesized and 58.2, 61.5, 81.4, and 85.4% by chemically synthesized NPs	[12]
	Chemical Precipitation	Indigo Carmine	0.75 g L^{-1}	100 mg L^{-1}	UV light	92%	[13]
	Chemical Precipitation	Chemical Oxygen Demand	0.75 g L^{-1}	-	UV light	74%	[13]
	Direct Precipitatio	Leather dye	0.5 mg mL^{-1}	300 mg L^{-1}	Sun light	90%	[14]

n						
Biosynthesized via *G. pulchellum* and chemically synthesized via NaOH as reducing agents	Congo red	0.1 g 10 mL^{-1}	50 ppm	-	100% by bio and 82% by chemically synthesized NPs	[15]
Gynostemma plant extract	Malachite green	200 mg L^{-1}	10 mg L^{-1}	UV light	89%	[16]
Punica granatum	Methylene blue	20 µg mL^{-1}	10 mg L^{-1}	UV light	93.4%	[17]
Chemically using NaOH as reducing agent	Methyl red	0.02 g	100 ppm	UV light	90%	[18]
Conocarpus erectus leaf extract	Congo red (CR) Methylene blue (MB)	0.5 mg mL^{-1}	50 ppm	UV and Sunlight	CR upto 97% MB upto 88% MG upto 90% RB5 upto 59%	Current study

		Malachite green (MG) Reactive black 5 (RB5) Reactive red 2 (RR2)				RR2 upto 57%	
	Chemically using NaOH as reducing agent	Congo red (CR) Methylene blue (MB) Malachite green (MG) Reactive black 5 (RB5) Reactive red 2 (RR2)	2 mg mL^{-1}	50 ppm	UV and Sunlight	CR upto 95% MB upto 75% MG upto 89% RB5 upto 46% RR2 upto 49%	Current study

170

171 **Table S2** Comparison of impact of ZnO-NPs on health of different crops with other studies

Catalysts	Plant	NPs Dosage	Stress	Impact	Reference
ZnO-NPs	*Oryza sativa* L. (Rice)	50 mg L^{-1}	Salinity	NaCl reduced the root, shoot length, cholophyll content,	[19]

			carotenoid, APX, and SOD contents while increased the MDA. The application of ZnO-NPs not only increases the growth and photosynthetic contents but also reduces the MDA, under salt stress.	
Lycopersicon esculentum (tomato)	50 mg L^{-1}	Cadmium	Cd (0.8 mM) decreased the shoot length by 28%, root length by 31%, shoot fresh mass by 32%, root fresh mass by 29%, shoot dry mass by 28%, root dry mass by 31%, and leaf area by 32%. The application of ZnO-NPs reduced the impact of Cd stress by increasing CAT by 51%, POX by 47%, and SOD by 51% activities. It also decreased the MDA, H_2O_2 and O^-_2 by 31%, 28%, and 31%	20
Cucumber	100 mg L^{-1}	Drought	Drought stress reduced the shoot fresh weight, dry weight,	21

			root fresh and dry weight by 25%, 55%, 59.35% and 41.65%. While ZnO-NPs at 100 mg L^{-1} ameliorate the drought stress by enhancing shoot fresh weight and dry weight, root fresh, and dry weight by 80.06%, 271.95%, 158.0%, and 104.45%.	
Pisum sativum L. (Pea)	50 and 100 mg L^{-1}	Drought	50 ppm of ZnO-NPs increased the growth, physiological, antioxidant, and mineral content by 35%, 45%, 57%, and 13% while 100 ppm enhanced it to 43%, 54%, 64%, and 15% under drought stress	[22]
Wheat	100 mg L^{-1}	Municipal wastewater	Under stress,100 mg $L^{-1}$of ZnO-NPs increased the SOD, POD, CAT, and APX by 55.4%, 26.7%, 48.5%, and 27.1%, as compared to control	[23]
Vigna radiata	100 mg L^{-1}	Textile wastewater	Significantly improved the health of crop by reducing the	Current study

References

1 L. M. Mahlaule-Glory and N. C. Hintsho-Mbita, Green derived zinc oxide (ZnO) for the degradation of dyes from wastewater and their antimicrobial activity: a review, *Catalysts*, 2022, **12**, 833.

2 M. Bagheri, N. R. Najafabadi and E. Borna, Removal of reactive blue 203 dye photocatalytic using ZnO nanoparticles stabilized on functionalized MWCNTs, *J. King Saud Univ.*, 2020, **32**, 799–804.

3 R. Farouq, E. K. Ismaeel and A. M. Monazie, Optimized degradation of eosin dye through UV-ZnO NPs catalyzed reaction, *J. Fluoresc.*, 2022, **32**, 715–722.

4 J. P. Shubha, H. S. Savitha, R. C. Patil, M. E. Assal, M. R. Shaik, M. Kuniyil, O. Alduhaish, N. Dubasi and S. F. Adil, A green approach for the degradation of toxic textile dyes by nickel oxide (NiO-SD) NPs: Photocatalytic and kinetic approach, *J. King Saud Univ.*, 2023, **35**, 102784.

5 T. Sarkar and A. Bhattacharjee, Green synthesized ZnO nanocatalysts for rapid and effective visible-light degradation of industrial dyes, *RSC Adv.*, 2026, **16**, 2671–2684.

6 H. Chelghoum, N. Nasrallah, H. Tahraoui, M. F. Seleiman, M. M. Bouhenna, H. Belmeskine, M. Zamouche, S. Djema, J. Zhang and A. Mendil, Eco-friendly synthesis of ZnO nanoparticles for quinoline dye photodegradation and antibacterial applications using advanced machine learning models, *Catalysts*, 2024, **14**, 831.

7 D. Mukhopadhyay, P. Gupta, R. Patidar and V. C. Srivastava, Microbial peroxide producing cell mediated lignin valorization, *Int. J. Biol. Macromol.*, 2022, **202**, 431–437.

8 F. Kanwal, T. Javed, F. Hussain, M. Wasim and M. Batool, Enhanced dye photodegradation through ZnO and ZnO-based photocatalysts doped with selective transition metals: a review, *Environ. Technol. Rev.*, 2024, **13**, 754–793.

9 N. Siva, D. Sakthi, S. Ragupathy, V. Arun and N. Kannadasan, Synthesis, structural, optical and photocatalytic behavior of Sn doped ZnO nanoparticles, *Mater. Sci. Eng. B*, 2020, **253**, 114497.

10 A. S. Al-Shehri, Z. Zaheer, A. M. Alsudairi and S. A. Kosa, Photo-oxidative Decolorization of Brilliant Blue with AgNPs as an Activator in the Presence of K2S2O8 and NaBH4, *ACS omega*, 2021, **6**, 27510–27526.

11 R. S. Das, B. Singh, A. Mandal, R. Banerjee and S. Mukhopadhyay, Homogeneous Palladium Nanoparticles Surface Hosts Catalyzed Reduction of the Chromophoric Azo (–N= N–) Group of Dye, Acid Orange 7 by Borohydride in Alkaline Media, *Int. J. Chem. Kinet.*, 2014, **46**, 746–758.

12 K. Siddique, M. Shahid, T. Shahzad, F. Mahmood, H. Nadeem, M. Saif ur Rehman, S. Hussain, O. Sadak, S. Gunasekaran and T. Kamal, Comparative efficacy of biogenic zinc oxide nanoparticles synthesized by Pseudochrobactrum sp. C5 and chemically synthesized zinc oxide nanoparticles for catalytic degradation of dyes and wastewater treatment, *Environ. Sci. Pollut. Res.*, 2021, **28**, 28307–28318.

13 R. S. Ahmed, H. M. Hameed, M. W. Muayad, C. N. Salih, U. M. Nayef, A. A. Abed, A. M. Hussien and A. Awad, Photocatalytic Degradation of Indigo Carmine by Zinc Oxide

Nanoparticles: Effect of Experimental Parameters and Kinetic Degradation, *Plasmonics*, 2025, 1–17.

14 V. Sharma, J. K. Sharma, V. Kansay, V. D. Sharma, A. Sharma, S. Kumar, A. K. Sharma and M. K. Bera, The effect of calcination temperatures on the structural and optical properties of zinc oxide nanoparticles and their influence on the photocatalytic degradation of leather dye, *Chem. Phys. Impact*, 2023, **6**, 100196.

15 M. A. Hassaan, S. Hosny, M. R. ElKatory, R. M. Ali, T. A. Rangreez and A. El Nemr, Dual action of both green and chemically synthesized zinc oxide nanoparticles: Antibacterial activity and removal of Congo red dye, *Desalin. Water Treat.*, 2021, **218**, 423–435.

16 J. K. Park, E. J. Rupa, M. H. Arif, J. F. Li, G. Anandapadmanaban, J. P. Kang, M. Kim, J. C. Ahn, R. Akter and D. C. Yang, Synthesis of zinc oxide nanoparticles from Gynostemma pentaphyllum extracts and assessment of photocatalytic properties through malachite green dye decolorization under UV illumination-A Green Approach, *Optik (Stuttg).*, 2021, **239**, 166249.

17 A. Fouda, E. Saied, A. M. Eid, F. Kouadri, A. M. Alemam, M. F. Hamza, M. Alharbi, A. Elkelish and S. E.-D. Hassan, Green synthesis of zinc oxide nanoparticles using an aqueous extract of punica granatum for antimicrobial and catalytic activity, *J. Funct. Biomater.*, 2023, **14**, 205.

18 T. Gul, I. Khan, B. Ahmad, S. Ahmad, A. A. Alsaiari, M. Almehmadi, O. Abdulaziz, A. Alsharif, I. Khan and K. Saeed, Efficient photodegradation of methyl red dye by kaolin clay supported zinc oxide nanoparticles with their antibacterial and antioxidant activities, *Heliyon*.

19 A. Singh, R. S. Sengar, V. D. Rajput, S. Agrawal, K. Ghazaryan, T. Minkina, A. R. M. Al Tawaha, O. M. Al Zoubi and T. Habeeb, Impact of zinc oxide nanoparticles on seed germination characteristics in rice (Oryza sativa L.) under salinity stress, *J. Ecol. Eng.*, 2023, **24**, 142–156.

20 M. Faizan, A. Faraz, A. R. Mir and S. Hayat, Role of zinc oxide nanoparticles in countering negative effects generated by cadmium in Lycopersicon esculentum, *J. Plant Growth Regul.*, 2021, **40**, 101–115.

21 M. I. Ghani, S. Saleem, S. A. Rather, M. S. Rehmani, S. Alamri, V. D. Rajput, H. M. Kalaji, N. Saleem, T. A. Sial and M. Liu, Foliar application of zinc oxide nanoparticles: An effective strategy to mitigate drought stress in cucumber seedling by modulating antioxidant defense system and osmolytes accumulation, *Chemosphere*, 2022, **289**, 133202.

22 A. Ishfaq, I. Haidri, U. Shafqat, I. Khan, M. Iqbal, F. Mahmood and M. U. Hassan, Impact of biogenic zinc oxide nanoparticles on physiological and biochemical attributes of pea (Pisum sativum L.) under drought stress, *Physiol. Mol. Biol. Plants*, 2025, **31**, 11–26.

23 A. Ishfaq, I. Haidri, U. Shafqat, I. Khan, H. M. Rizwan, M. U. Hassan, M. Irfan, M. Adnan and F. Mahmood, Microbial Synthesis of ZnO Nanoparticles: A Green Strategy for Mitigating Wastewater Stress in Wheat (Triticum aestivum), *Water, Air, Soil Pollut.*, 2025, **236**, 518.